

The Simple Cubic Lattice of Superparamagnetic Nanoparticles: The Role of Interparticle Correlations

Sergey A. Sokolsky,¹ Anna Yu. Solovyova,¹ and Ekaterina A. Elfimova^{1,*}

¹*Ural Mathematical Center, Ural Federal University,
51 Lenin Avenue, Ekaterinburg 620000, Russia*

(Dated: August 30, 2022)

In this work, we study the effect of dipole-dipole interparticle interactions on the static thermodynamic and magnetic properties of an ensemble of immobilized monodisperse superparamagnetic particles. We assume that magnetic particles are embedded on the nodes of the regular cubic lattice so, that particle translational degrees of freedom are turned out. The relaxation of the magnetic moments of the particles occurs by the Néel mechanism. The easy axes are distributed according to the particular textures: these are (i) aligned parallel or (ii) perpendicular to the direction of an external field. This model is studied using both theory and computer simulation taking microscopic discrete structure explicitly into account. The theory is based on the Helmholtz free energy expansion like classical virial series up to the second virial coefficient. The analytical predictions for the Helmholtz free energy, the magnetization, and the initial magnetic susceptibility are calculated for both texturing types (i) and (ii) as functions of the height of the magnetic crystallographic anisotropy energy barrier for internal superparamagnetic rotation of magnetic moments inside the particles. The obtained theoretical results describing the model system are compared against Monte-Carlo simulation data.

I. INTRODUCTION

Smart materials, called also responsive or intelligent materials, are special materials that have one or more properties that can be significantly changed in a controlled fashion by external stimuli, for example magnetic field. Such materials include magnetic composites which is produced by embedding magnetic nanoparticles in liquid or polymer matrix. The examples of these composites are ferrofluids, magnetic elastomers, ferrogels, magnetic emulsions, and various biocompatible magnetic filling [1–4]. Nowadays, such materials are widely used in various medical applications because of the ability to actively respond to applied magnetic field. For example, they are an indispensable tool in magnetic hyperthermia, in which micromotions of ferroparticles in an alternating magnetic field leads to heating and destruction of tumor cells [5–8]. The response of the magnetic composites to the applied magnetic field is determined by two main physical mechanisms of the magnetic moment orientational relaxation in nanosized particles. They are the Brownian rotation of particles with fixed magnetic moments and the superparamagnetic Néel rotation of the magnetic moments inside the particles due to thermal fluctuations [9–11]. For ensemble of nanoparticles, suspended in some liquid carriers, known as ferrofluids, both mechanisms take place. But in the case, when particles are embedded in some polymer matrix or biological tissues, the particles often lose their translational and orientational degrees of freedom. In this case, the superparamagnetic Néel relaxation becomes the major mechanism determining the magnetic properties of the ensembles of such immobilized particles.

Nowadays there exist many established synthesis techniques that make it possible to generate magnetic composite with different microscopic architecture [4, 12–14]. A different distribution of magnetic particles inside the sample leads to a significant change in its bulk properties [15–17]. In addition, interparticle dipole-dipole interactions have a strong effect on the macroproperties of the system, and this is manifested differently in liquid or polymer based composites. So, the strong interparticle dipole-dipole interactions lead to aggregation in the ferrofluid [18–21], whereas in the system of immobilized ferroparticles the interparticle interactions can only be a cause of the structuring of the magnetic moments of the particles, since the particles themselves remain stationary [22–24]. The effects of dipole-dipole interactions on the bulk properties of ferrofluids are well understood theoretically [25–28], experimentally [29, 30], and by computer simulation methods [27, 28, 31], while the theory of the effect of interactions on immobilized superparamagnetic particles still remains a challenge.

In our recent studies, using statistical-mechanical theory and computer simulations, we investigated magnetic response of the system of immobilized interacting single-domain particles distributed randomly [17] or placed at the nodes of a simple cubic lattice [24] within an implicit solid matrix. In the first work [17] superparamagnetic particles with uniaxial magnetic anisotropy were considered. The relaxation of the magnetic moments of particles occurs by the Néel mechanism. The easy axes were distributed according to the particular textures: these are aligned parallel or perpendicular to an external magnetic field, or randomly distributed. The initial magnetic susceptibility was found to depend on magnetic crystallographic anisotropy barrier (measured with respect to the thermal energy by a parameter σ) in very different ways for various texture. With a parallel texture, the initial

* ekaterina.elfimova@urfu.ru

susceptibility increases with increasing σ , while with a perpendicular texture, the initial susceptibility decreases. With a random distribution, the initial susceptibility is independent on σ . In all cases, including interactions between particles leads to an enhancement of the initial susceptibility, but the enhancement is much stronger for the parallel texture than for the perpendicular or random textures. In the second work [24] we assumed that ferroparticles are embedded on the nodes of the simple cubic lattice (SCLF) and can rotate at lattice nodes under the influence of an external magnetic field and as a result of the interparticle dipole-dipole interactions; however, particle translational degrees of freedom are turned off. Two types of real magnetic composites correspond to this model. In the first case, particles have a rigid connection with the carrier matrix and they are characterized by a Néel mechanism of the magnetic moment relaxation. However, the internal magnetic anisotropy of particles in this case is low and the magnetic moment can freely rotate inside the particle body. Typically, the size of such particles is small and the dipole-field relationship turns out quite weak. In the second case, particles can rotate in some "caverns" of the host medium and the orientation of the magnetic moment changes according to the Brownian mechanism. Usually such particles have a large size and react strongly with the field. The magnetic properties of SCLF and ferrofluid, modeled by a system of dipole hard spheres (DHS), were compared. It has been found that at low intensities of the dipole-dipole interaction the magnetization of DHS and SCLF is the same. For strong and moderate dipolar coupling regime and at the weak magnetic field, the magnetization of the DHS system is higher than the magnetization of SCLF, while the opposite tendency is observed at stronger fields. The reasons of this behavior were discussed in the article [24].

These two works [17, 24] provided deep and important information about the relationship between microstructure and macroproperties of the magnetic composites. Nevertheless, the theory is still incomplete and the topic is not fully understood. The aim of this work is to combine previous research and study a new model – a monodisperse system of immobilized interacting single-domain spherical ferroparticles, with uniaxial magnetic anisotropy, placed at the nodes of a simple cubic lattice.

This article is organized as follows. In section II, the model system is given, the results of the Helmholtz free energy expansion are described, and simulation details are summarized. The results of a comparison of the new theory with simulation data are discussed in section III. Section IV concludes the article.

II. MODEL AND METHODS

A. Model

The sample under consideration is the monodisperse system of N immobilized superparamagnetic spherical nanoparticles placed at the nodes of the simple cubic lattice with period a . All particles have the same magnetic-core diameter x and magnetic moment $m = v_m M_s$, where M_s is the bulk saturation magnetization, $v_m = \pi x^3/6$ is the magnetic core volume. The radius vector and magnetic moment of particle i are $\mathbf{r}_i = r_i \hat{\mathbf{r}}_i$ and $\mathbf{m}_i = m_i \boldsymbol{\Omega}_i$ respectively, where $\hat{\mathbf{r}}_i = (\sin \theta_i \cos \phi_i, \sin \theta_i \sin \phi_i, \cos \theta_i)$ and $\boldsymbol{\Omega}_i = (\sin \omega_i \cos \xi_i, \sin \omega_i \sin \xi_i, \cos \omega_i)$ are unit vectors.

The magnetic moment of a particle has two degenerate ground-state directions, these being parallel and anti-parallel to the easy axis, denoted by the vector \mathbf{n}_i . The Nel energy U_N as a function of the angle between \mathbf{m}_i and \mathbf{n}_i is given by

$$U_N(i) = -K v_m (\boldsymbol{\Omega}_i \cdot \hat{\mathbf{n}}_i)^2, \quad (1)$$

where $\hat{\mathbf{n}}_i$ is a unit vector, K is the magnetic crystallographic anisotropy constant (a material property).

The interaction between magnetic moment \mathbf{m}_i and uniform external magnetic field \mathbf{H} is described by Zeeman energy

$$U_m(i) = -\mu_0 (\mathbf{m}_i \cdot \mathbf{H}) = -\mu_0 m H (\boldsymbol{\Omega}_i \cdot \hat{\mathbf{h}}), \quad (2)$$

where assumed that the applied magnetic field \mathbf{H} has the strength H and the orientation $\hat{\mathbf{h}}$.

The magnetic interaction between particles i and j is defined by the anisotropic dipole-dipole interaction U_d

$$U_d(ij) = \frac{\mu_0 m^2}{4\pi r_{ij}^3} \left[(\boldsymbol{\Omega}_i \cdot \boldsymbol{\Omega}_j) - 3(\boldsymbol{\Omega}_i \cdot \hat{\mathbf{r}}_{ij})(\boldsymbol{\Omega}_j \cdot \hat{\mathbf{r}}_{ij}) \right], \quad (3)$$

where $\mathbf{r}_{ij} = r_{ij} \hat{\mathbf{r}}_{ij} = \mathbf{r}_j - \mathbf{r}_i$ is the interparticle separation vector and $r_{ij} = |\mathbf{r}_{ij}|$.

The total interaction energy can be written in units of the thermal energy $k_B T = \beta^{-1}$ as

$$\beta U = \beta \sum_{j>i=1}^N U_d(ij) - \sigma \sum_{i=1}^N (\boldsymbol{\Omega}_i \cdot \hat{\mathbf{n}}_i)^2 - \alpha \sum_{i=1}^N (\boldsymbol{\Omega}_i \cdot \hat{\mathbf{h}}), \quad (4)$$

where the dimensionless anisotropy parameter $\sigma = \beta v_m K$ and Langevin parameter $\alpha = \beta \mu_0 m H$ are introduced. Since the distance between particles i and j can be no smaller than the lattice period $a \geq x$, it is convenient to introduce the effective dipolar coupling constant λ_e for cubic lattice as follows

$$\lambda_e = \frac{\mu_0 m^2 \beta}{4\pi a^3}, \quad (5)$$

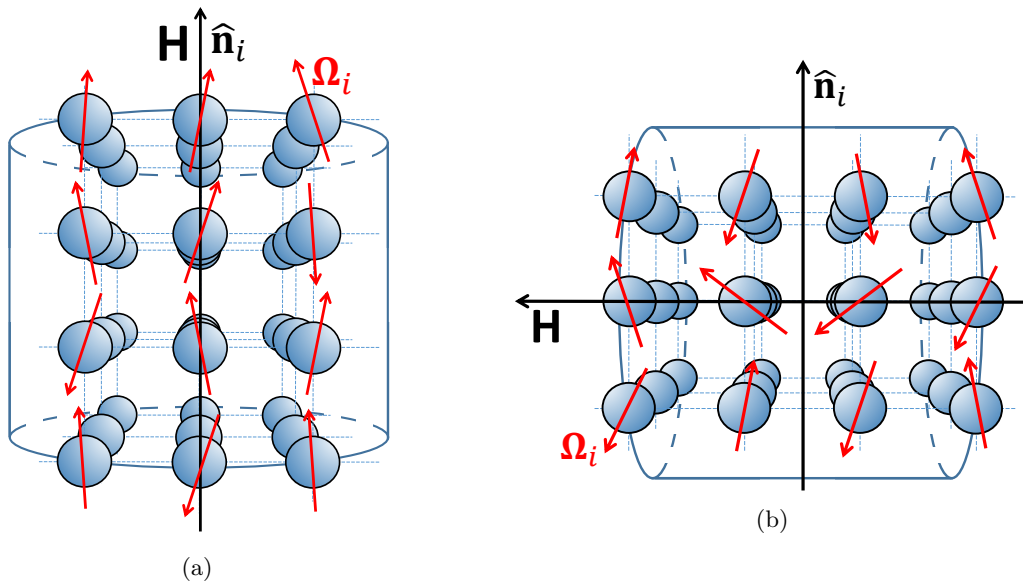


FIG. 1. Monodisperse system of immobilized single-domain superparamagnetic ferroparticles placed at the nodes of a simple cubic lattice at external magnetic field for (a) parallel and (b) perpendicular configurations.

which measures the importance of the magnetic interaction of two particles located in neighboring nodes of the lattice as compared to the thermal energy. Two types of orientational distributions of the easy axes will be considered: aligned (i) parallel and (ii) perpendicular to the direction of an external field \mathbf{H} . To simplify analytical calculations, easy axes of both configuration are assumed to be aligned along the laboratory Oz axis namely $\hat{\mathbf{n}}_i = (0, 0, 1)$, so the Neel energy can be represented as

$$U_N(i) = -\sigma \cos^2 \omega_i. \quad (6)$$

The direction of external magnetic field \mathbf{H} is set (i) $\mathbf{H} = H(0, 0, 1)$ in parallel configuration so that

$$U_m^{\parallel}(i) = -\alpha \cos \omega_i \quad (7)$$

and (ii) $\mathbf{H} = H(1, 0, 0)$ in perpendicular configuration so

$$U_m^{\perp}(i) = -\alpha \sin \omega_i \cos \xi_i. \quad (8)$$

For vanishing of demagnetization fields, we will assume that the sample container has a long cylindrical shape elongated in the direction of an external magnetic field \mathbf{H} . The sample geometries studied in this work are given in Fig. 1.

B. The Helmholtz Free Energy of ensemble of immobilized particles

1. Ideal system

The Helmholtz free energy F of the SCLF at external magnetic field can be presented via configurational

integral Z as follows

$$\beta F = -\ln(Z). \quad (9)$$

To extract the contribution of the dipole-dipole interaction it is convenient to split the Helmholtz free energy F into two parts

$$F = F_{\text{id}} + \Delta F. \quad (10)$$

The first term corresponds the system of an ideal superparamagnetic non-interacting particles, the configurational integral Z_{id} of which is

$$\beta F_{\text{id}} = -\ln(Z_{\text{id}}), \quad (11)$$

$$Z_{\text{id}} = \prod_{k=1}^N \int p(\mathbf{r}_k) d\mathbf{r}_k d\Omega_k \times \exp\left(\sum_{i=1}^N [\alpha(\Omega_i \cdot \hat{\mathbf{h}}) + \sigma \cos^2 \omega_i]\right), \quad (12)$$

$$d\mathbf{r}_k = r_k^2 \sin \theta_k dr_k d\theta_k d\phi_k, \quad (13)$$

$$d\Omega_k = \frac{1}{4\pi} \sin \omega_k d\omega_k d\xi_k. \quad (14)$$

In this definition $p(\mathbf{r}_k)$ is the probability distribution function of the position of particle k

$$p(\mathbf{r}_k) = \delta(\mathbf{r}_k - \mathbf{r}_k^{(0)}), \quad (15)$$

where $\mathbf{r}_k^{(0)}$ is the 'lattice position' of particle k which can be in a crystalline lattice, or in a random configuration. In all cases, the normalization condition is

$$\int p(\mathbf{r}_k) d\mathbf{r}_k = 1. \quad (16)$$

Therefore in Eq. (12), the integrand function depends only on the orientation of the magnetic moments. With this integration, all particles are equivalent to each other. This allows us to rewrite Z_{id} as follows

$$Z_{\text{id}} = \left(\int d\Omega_1 \exp \left[\alpha(\Omega_1 \cdot \hat{\mathbf{h}}) + \sigma \cos^2 \omega_1 \right] \right)^N, \quad (17)$$

the result of which can be calculated numerically for each set of parameters α and σ and fixed direction of vector $\hat{\mathbf{h}}_1$. It worth be stressed, that the Helmholtz free energy of ideal system

$$\frac{\beta F_{\text{id}}}{N} = -\ln \left(\int d\Omega_1 \exp \left[\alpha(\Omega_1 \cdot \hat{\mathbf{h}}) + \sigma \cos^2 \omega_1 \right] \right) \quad (18)$$

does not depend on parameter λ , which characterizes the dipole-dipole interparticle interactions.

2. System with interparticle dipole-dipole interactions

The last term ΔF in (10) is defined via the ratio of the configurational integral of the SCLF, including dipole-dipole interaction Z and the configurational integral of an ideal paramagnetic system of non-interacting particles Z_{id}

$$\beta \Delta F = -\ln \left(\frac{Z}{Z_{\text{id}}} \right), \quad (19)$$

$$\frac{Z}{Z_{\text{id}}} = \frac{1}{Z_{\text{id}}} \prod_{k=1}^N \int p(\mathbf{r}_k) d\mathbf{r}_k d\Omega_k \exp \left(-\beta \sum_{j>i=1}^N U_d(ij) + \sum_{i=1}^N [\alpha(\Omega_i \cdot \hat{\mathbf{h}}) + \sigma \cos^2 \omega_i] \right), \quad (20)$$

Using the Boltzmann-weighted integration over the orientation of particle i

$$d\Psi_k = \frac{d\Omega_k \exp \left[\alpha(\Omega_k \cdot \hat{\mathbf{h}}) + \sigma \cos^2 \omega_k \right]}{\int d\Omega_1 \exp \left[\alpha(\Omega_1 \cdot \hat{\mathbf{h}}) + \sigma \cos^2 \omega_1 \right]}, \quad (21)$$

it is possible to reduce definition (20) as

$$\frac{Z}{Z_{\text{id}}} = \prod_{k=1}^N \int p(\mathbf{r}_k) d\mathbf{r}_k d\Psi_k \prod_{j>i=1}^N (1 + f_{ij}), \quad (22)$$

$$f_{ij} = \exp(-\beta U_d(ij)) - 1, \quad (23)$$

where f_{ij} is the Mayer function. This approach is reproduced the method of [24], which was developed for $\sigma \equiv 0$. The main difference is the definition of the Boltzmann-weighted integration $d\Psi_k$ (21), which in our case also depends on the anisotropy parameter $\sigma \geq 0$ and coincides with the same from [24] for $\sigma = 0$. Therefore, it is possible to apply the final results for configurational part of the Helmholtz free energy from [24] to our system with the new definition of operator $d\Psi_k$:

$$\frac{\beta \Delta F}{N} = -\frac{1}{2} \sum_{j=2}^N \langle f_{1j}^{(0)} \rangle. \quad (24)$$

where $f_{1j}^{(0)} = \int p(\mathbf{r}_1) d\mathbf{r}_1 \int p(\mathbf{r}_j) d\mathbf{r}_j f_{1j}$ is the Mayer function in the 'lattice position' of particles 1 and j . The angle brackets mean a Boltzmann-weighted average (21) over the orientation of each particles involved

$$\langle f_{1j}^{(0)} \rangle = \int f_{1j}^{(0)} d\Psi_1 d\Psi_j. \quad (25)$$

It should be emphasized that approximation (24) is obtained up to the linear term of the logarithm expansion (19) and it takes into account interparticle interactions in all ferroparticle pairs that corresponds with the second virial coefficient level.

This definition of ΔF is valid for the regular types of particle distribution in the system volume, such as SCLF or other types of lattices. For the random distribution of ferroparticles in sample volume it is necessary to average (24) over all possible random configurations. It means that in the limit every particle j in sum of (24) can occupy any position in the sample volume except the position of particle 1:

$$\begin{aligned} \frac{\beta \Delta F^{\text{random}}}{N} &= -\frac{1}{2} \sum_{j=2}^N \int \frac{dr_{1j}}{V} \langle f_{1j} \rangle \\ &= -\frac{N}{2V} \int dr_{12} \langle f_{12} \rangle = \rho B_2, \end{aligned}$$

where $\rho = N/V$ is nanoparticle density, B_2 corresponds the classical definition of the second virial coefficient in the theory of liquids [32].

Next we will consider in detail the behavior of SCLF. So, the Mayer function (23) is expanded into a series over the powers of dipolar energy up to U_d^3

$$f_{1j}^{(0)} = -\beta U_d(1j) + \frac{[-\beta U_d(1j)]^2}{2!} + \frac{[-\beta U_d(1j)]^3}{3!}. \quad (26)$$

Dipole-dipole potential U_d depends on the radius vector \mathbf{r}_{1j} of particles 1 and j and the magnetic moments \mathbf{m}_1 and \mathbf{m}_j . After the Boltzmann-weighted averaging over the orientation of magnetic moments \mathbf{m}_1 and \mathbf{m}_j one can represent the value of $\beta \Delta F$ in the common form

$$\frac{\beta \Delta F}{N} = -\frac{1}{2} (b_1 \lambda_e + b_2 \lambda_e^2 + b_3 \lambda_e^3), \quad (27)$$

$$b_1 = \sum_{j=2}^N \left\langle \frac{-\beta U_d(1j)}{\lambda_e} \right\rangle, \quad (28)$$

$$b_2 = \sum_{j=2}^N \left\langle \frac{1}{2!} \left(\frac{-\beta U_d(1j)}{\lambda_e} \right)^2 \right\rangle, \quad (29)$$

$$b_3 = \sum_{j=2}^N \left\langle \frac{1}{3!} \left(\frac{-\beta U_d(1j)}{\lambda_e} \right)^3 \right\rangle. \quad (30)$$

The coefficients b_1 , b_2 and b_3 are different for parallel and perpendicular configurations and will be discussed for each case separately.

C. Parallel configuration of SCLF with superparamagnetic nanoparticles

Parallel configuration corresponds to the illustration in Fig. 1 (a), that means $(\boldsymbol{\Omega}_i \cdot \hat{\mathbf{h}}) = (\boldsymbol{\Omega}_i \cdot \hat{\mathbf{n}}_i) = \cos \omega_i$. In this case the ideal part of the Helmholtz free energy (18) is equal to

$$\frac{\beta F_{\text{id}}}{N} = -\ln [Q_0(\alpha, \sigma)], \quad (31)$$

where

$$Q_0(\alpha, \sigma) = \frac{1}{2} \int_{-1}^1 \exp(\alpha t + \sigma t^2) dt, \quad (32)$$

$$Q_0(\alpha, 0) = \frac{\sinh \alpha}{\alpha}. \quad (33)$$

The Boltzmann-weighted integration over the orientation of particle magnetic moment for parallel configuration looks like

$$d\Psi_k = \frac{d\boldsymbol{\Omega}_k \exp(\alpha \cos \omega_k + \sigma \cos^2 \omega_k)}{Q_0(\alpha, \sigma)}. \quad (34)$$

Details of the averaging of the coefficients b_1, b_2, b_3 over magnetic moment orientations and particle positions are derived in Appendix A. The final analytical expression for ΔF expansion can be presented as

$$\begin{aligned} \frac{\beta \Delta F}{N} = & -2.0944 Q_1^2(\alpha, \sigma) \lambda_e \\ & - [1.9390 Q_2^2(\alpha, \sigma) + 1.4003] \lambda_e^2 \\ & - [0.1611 Q_3^2(\alpha, \sigma) + 1.5595 Q_1(\alpha, \sigma) Q_3(\alpha, \sigma) \\ & - 0.7285 Q_1^2(\alpha, \sigma)] \lambda_e^3, \end{aligned} \quad (35)$$

where additional functions $Q_k(\alpha, \sigma)$ are defined in Appendix A. It is well known that the virial expansion for a system with dipole-dipole interactions is an alternating series [33, 34], and therefore it is very sensitive to truncation of the series. Hence, it could be more efficient to transform the virial expansion of the Helmholtz free energy (35) back into the logarithmic form (19):

$$\begin{aligned} \frac{\beta \Delta F}{N} = & -\ln \left\{ 1 + 2.0944 Q_1^2(\alpha, \sigma) \lambda_e \right. \\ & + [1.9390 Q_2^2(\alpha, \sigma) + 1.4003] \lambda_e^2 \\ & + [0.1611 Q_3^2(\alpha, \sigma) + 1.5595 Q_1(\alpha, \sigma) Q_3(\alpha, \sigma) \\ & \left. - 0.7285 Q_1^2(\alpha, \sigma)] \lambda_e^3 \right\}, \end{aligned} \quad (36)$$

so that the terms from the right-hand side of the Eq. (35) are the first terms of the Maclaurin expansion of the logarithm in (36). The advantage of the logarithmic form is that the logarithm of a polynomial is less sensitive to polynomial truncation at the low order in λ_e -expansion. This method was first suggested in [35] and turned out to be capable of considerably expanding the

theory's applicability range over concentration and intensity of the interparticle dipole-dipole interactions for describing thermodynamic and magnetic properties of the dipolar hard sphere fluid [24, 36, 37]. The typical behavior of the dipole-dipole contribution in the Helmholtz free energy ΔF as a function of the anisotropy parameter σ is shown in Fig. 2 with $\alpha = 0, 1, 2$, and 5, and a rather large value of intensity of dipole-dipole interactions $\lambda_e = 0.5$. For $0 \leq \sigma \leq 5$ one can note more fast increasing of contribution ΔF than the same for $\sigma > 5$. In parallel configuration, anisotropy axes play a role addition stimulus to alignment of magnetic moments along the external magnetic field, that leads to increasing of the Helmholtz free energy with increasing anisotropy pa-

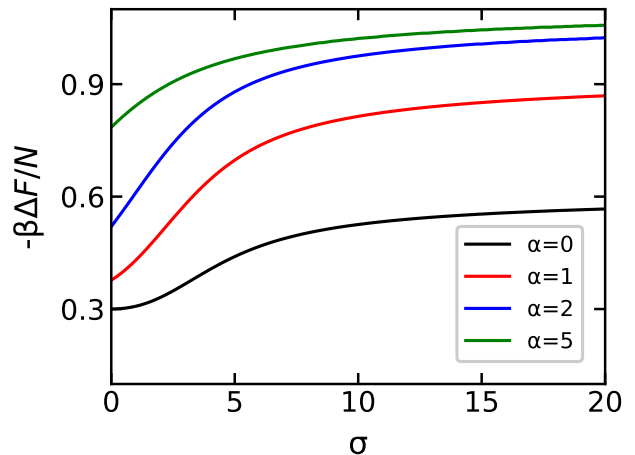


FIG. 2. The contribution of the dipole-dipole interactions ΔF for parallel configuration as a function of the anisotropy parameter σ for the system with $\lambda_e = 0.5$ and different value of $\alpha = 0, 1, 2$, and 5. The value of α grows from the bottom to the top.

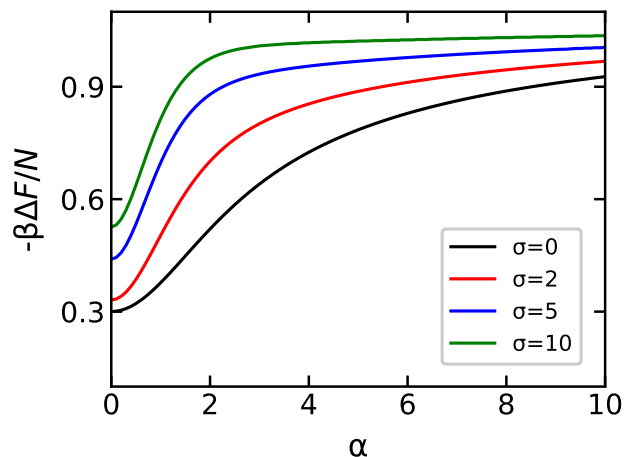


FIG. 3. The contribution of the dipole-dipole interactions ΔF for the parallel configuration as a function of the Langevin parameter α for the system with $\lambda_e = 0.5$ and different value of $\sigma = 0, 2, 5$ and 10. The value of σ grows from the bottom to the top.

parameter σ . The dependence of ΔF from the intensity of the external magnetic field is shown in Fig. 3 with $\sigma = 0, 2, 5$, and 10 , and $\lambda_e = 0.5$. The contribution ΔF is more sensitive to change of anisotropy parameter in intermediate magnetic fields $1 \leq \alpha \leq 5$, whereas at $\alpha \simeq 10$ different between values of ΔF with grows of σ is not sensitive.

D. Perpendicular configuration of SCLF with superparamagnetic nanoparticles

Perpendicular configuration is illustrated in Fig. 1 (b), that corresponds $(\mathbf{\Omega}_i \cdot \hat{\mathbf{h}}) = \sin \omega_i \cos \xi_i$. In this case the ideal part of the Helmholtz free energy (18) is equal to

$$\frac{\beta F_{\text{id}}}{N} = -\ln [R_0(\alpha, \sigma)], \quad (37)$$

where

$$R_0(\alpha, \sigma) = \int_0^1 \exp(\sigma t^2) I_0(\alpha \sqrt{1-t^2}) dt, \quad (38)$$

$$R_0(\alpha, 0) = \frac{\sinh \alpha}{\alpha}. \quad (39)$$

Here $I_0(x)$ is the modified Bessel function of zero order.

The Boltzmann-weighted integration over the orientation of particle magnetic moment for perpendicular configuration looks like

$$d\Psi_k = \frac{d\mathbf{\Omega}_k \exp(\alpha \sin \omega_k \cos \xi_k + \sigma \cos^2 \omega_k)}{R_0(\alpha, \sigma)}. \quad (40)$$

Details of the averaging of the coefficients b_1, b_2, b_3 over magnetic moment orientations and particle positions are derived in Appendix B. The final analytical expression for ΔF in the logarithmic form is

$$\begin{aligned} \frac{\beta \Delta F}{N} = & -\ln \left\{ 1 + 2.0944 R_1^2(\alpha, \sigma) \lambda_e \right. \\ & + [1.4542 R_2^2(\alpha, \sigma) + 4.3627 R_3^2(\alpha, \sigma) \\ & - 2.9085 R_3(\alpha, \sigma) + 1.8851] \lambda_e^2 \\ & + [2.8736 R_4(\alpha, \sigma) R_5(\alpha, \sigma) \\ & - 0.1429 R_4(\alpha, \sigma) R_6(\alpha, \sigma) \\ & + 0.2454 R_5(\alpha, \sigma) R_6(\alpha, \sigma) \\ & - 1.3856 R_4^2(\alpha, \sigma) - 0.4960 R_5^2(\alpha, \sigma) \\ & \left. - 1.3856 R_6^2(\alpha, \sigma)] \lambda_e^3 \right\}. \quad (41) \end{aligned}$$

Functions $R_k(\alpha, \sigma)$ are defined in Appendix B.

The dependence of the dipole-dipole contribution in the Helmholtz free energy ΔF as a function of the anisotropy parameter σ is shown in Fig. 4 with $\alpha = 0, 1, 2$, and 5 , and $\lambda_e = 0.5$. It should be noted that these dependencies are not monotonic except case for $\alpha = 0$ (black curve). In the area of low values of anisotropy parameter the increase of magnetic field intensity leads

to increasing of the dipole-dipole contribution in the Helmholtz free energy, but than all curves coincide with each other and show constant value for $\sigma \geq 8$. It means that for perpendicular configuration the dipolar part of the Helmholtz free energy ΔF for model system with $\sigma \gg 0$ depends mainly on the intensity of dipolar interaction λ and almost independent of α and σ . This fact can be found also from Fig. 5, where the ΔF is shown as a function of α . At $\sigma = 10$ (green curve) the behavior of ΔF is not very sensitive to increasing of the Langevin parameter.

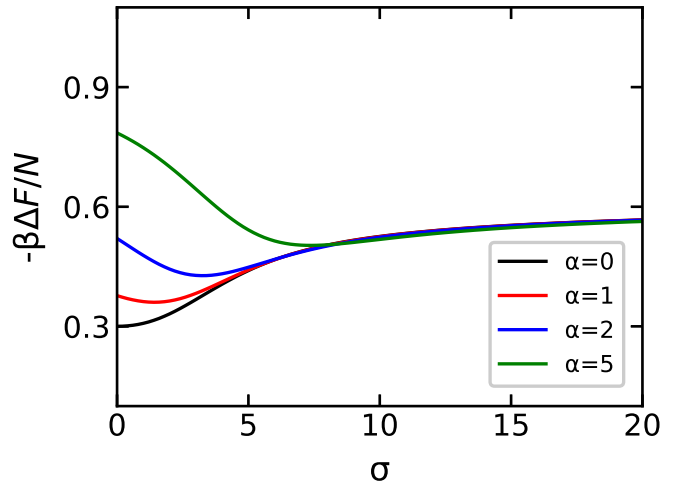


FIG. 4. The contribution of the dipole-dipole interactions ΔF for perpendicular configuration as a function of the anisotropy parameter σ for the system with $\lambda_e = 0.5$ and different value of $\alpha = 0, 1, 2$, and 5 . The value of α grows from bottom to top.

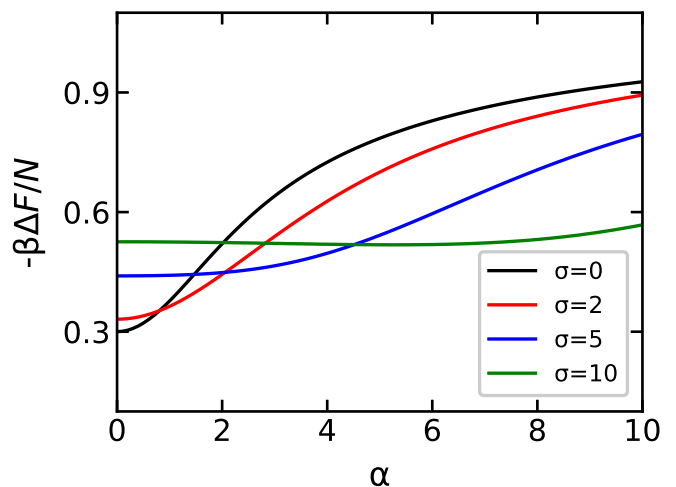


FIG. 5. The contribution of the dipole-dipole interactions ΔF for perpendicular configuration as a function of the Langevin parameter α for the system with $\lambda_e = 0.5$ and different value of $\sigma = 0, 2, 5$, and 10 .

E. Simulation

In order to check the accuracy of the new theory and find the range of its applicability, we thoroughly tested their predictions against computer simulation data obtained for a model system. Monte Carlo (MC) simulations were carried out in the canonical (NVT) ensemble. The modeled system consisted of $N = 512$ identical ferroparticles rigidly fixed at the lattice nodes inside a cubic simulation cell with 3D periodic boundary conditions imposed. To vanish all demagnetization effects the Ewald summation with conducting boundary conditions was used for computing the long-range dipole-dipole interactions between ferroparticles. It was assumed that the external magnetic field was directed along the Oz axis. The easy axes were unit vectors parallel to (i) the laboratory Oz axis in parallel configuration and (ii) the laboratory Ox axis in perpendicular configuration. To overcome the anisotropy barrier for large values of σ , there were two equiprobable types of rotational move: the ordinary random displacement and a flip move $\mathbf{m} \rightarrow -\mathbf{m}$ [17]. Typical run lengths consisted of 10^6 attempted rotations per particle after equilibration. Estimates of statistical errors were calculated using the blocking procedure described in [38]. In all cases, the obtained values of statistical errors does not exceed the size of symbols using for simulation data on the plots.

The Helmholtz free energy can not to be measured by numerical method directly, therefore its derivatives (the scalar magnetization and the initial magnetic susceptibility) were used to investigation the validity of the new theory. For both parallel and perpendicular configurations, the fractional magnetization was computed in the simulation as

$$M = \frac{1}{N} \left\langle \sum_{i=1}^N \cos \omega_i \right\rangle_t, \quad (42)$$

where $\langle \dots \rangle_t$ means the average over simulation time. The initial magnetic susceptibility was calculated at $\alpha = 0$ in the z direction only:

$$\chi = \chi_L \left\langle \left(\sum_{i=1}^N \cos \omega_i \right)^2 \right\rangle_t \frac{3}{N}, \quad (43)$$

where the Langevin susceptibility χ_L can be express via parameter λ_e using the relation $\rho = 1/a^3$ for the simple cubic lattice

$$\chi_L = \frac{4\pi\mu_0\rho m^2}{3k_B T} = \frac{4\pi}{3}\lambda_e. \quad (44)$$

To check the simulation algorithm with large values of anisotropy parameter, the ideal system of superparamagnetic ferroparticles was modeled where interparticle interaction turned off. In this case the exact theoretical results are known:

$$M_{\text{id}} = -\frac{\partial}{\partial \alpha} \left(\frac{\beta F_{\text{id}}}{N} \right), \quad (45)$$

$$\chi_{\text{id}} = -\frac{1}{V} \left. \frac{\partial^2 F_{\text{id}}}{\partial H^2} \right|_{H=0}, \quad (46)$$

where F_{id} is defined by (31) for parallel configuration and (37) for perpendicular configuration. In Fig. 6 and 7 one can find the excellent agreement between obtained sim-

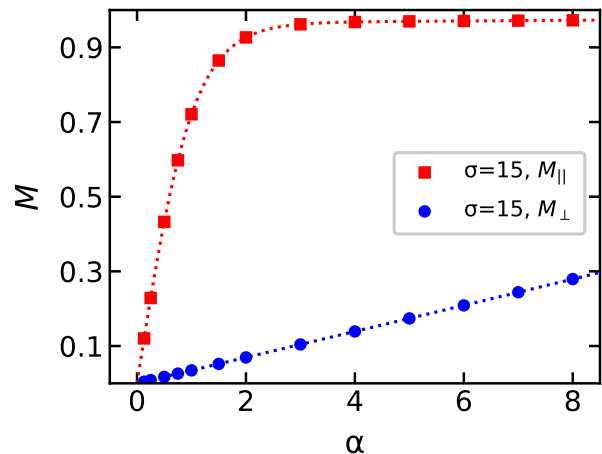


FIG. 6. The static magnetization as a function of the Langevin parameter α for system with $\sigma = 15$ in the absence of interparticle interactions. Dashed lines correspond ideal approximation (45). Symbols are from Monte-Carlo simulations. Results are shown for parallel (red squares and line) and perpendicular (blue circles and line) configurations.

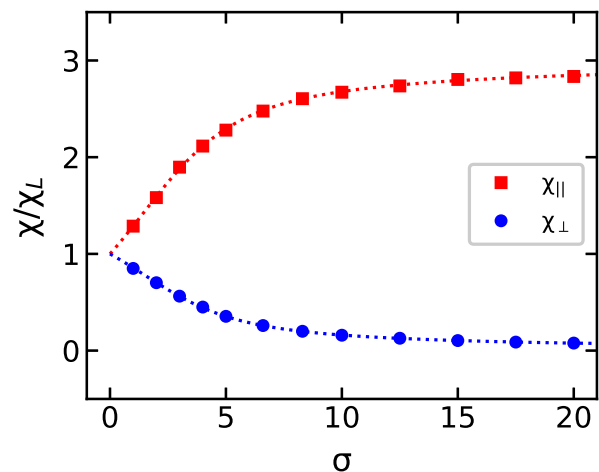


FIG. 7. The initial magnetic susceptibility χ divided by the Langevin susceptibility χ_L as a function of the anisotropy parameter σ for system without interparticle interactions. Dashed lines correspond ideal approximation (46). Symbols are from Monte-Carlo simulations. Results are shown for parallel (red squares and lines) and perpendicular (blue circles and lines) configurations.

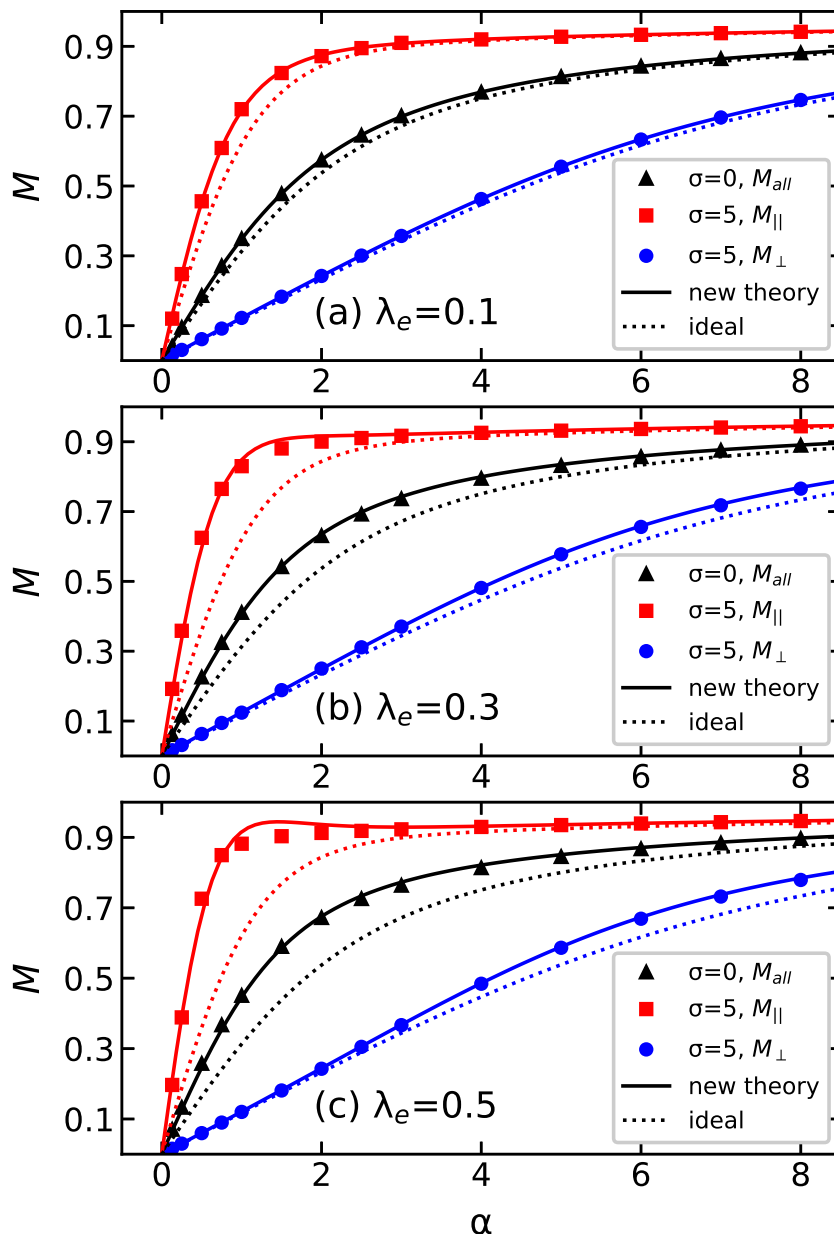


FIG. 8. The static magnetization as a function of the Langevin parameter α for systems with (a) $\lambda_e = 0.1$, (b) 0.3 and (c) 0.5. Solid lines correspond new theories for M_{\parallel} and M_{\perp} , dashed lines are ideal approximation (45). Symbols are from Monte-Carlo simulations. Results are shown for parallel (red squares and lines) and perpendicular (blue circles and lines) configurations with $\sigma = 5$ and for system with $\sigma = 0$ (black triangles and lines).

ulation data and ideal approximations (45) and (46) for both magnetization and the initial magnetic susceptibility.

III. RESULTS

The analytical expression of the Helmholtz free energy allows us to obtain predictions for various magnetic and thermodynamic properties of the system. So, the scalar magnetization is defined by

$$M = M_{id} - \frac{\partial}{\partial \alpha} \left(\frac{\beta \Delta F}{N} \right), \quad (47)$$

where ΔF can be found from (36) for parallel configuration and (41) for perpendicular configuration. The second term takes into account the interparticle dipole-dipole interactions in model system. Three systems were considered: with $\lambda_e = 0.1, 0.3$, and 0.5 . The Langevin susceptibilities for these systems are equal to $\chi_L = 0.42, 1.26$, and 2.1 respectively. In Fig. 8 theoretical static

magnetization curves are compared with MC simulation data. For $\sigma = 0$ (black curves), the theoretical predictions for both parallel and perpendicular configurations are coincident with each other, that was expected. In this case it should be noted the excellent agreement of the new theory (solid lines) with the simulation data for all considered systems, whereas the ideal approximation (dashed lines) works quite good only for system with a weak interactions ($\lambda_e = 0.1$). The same can be said about the perpendicular configuration with $\sigma = 5$ (blue curves). The magnetization of the parallel configuration with $\sigma = 5$ increases rapidly with increasing of the magnetic field intensity, and the dipole-dipole interaction effect is more pronounced in this case. However for $\sigma = 5$ and $\lambda_e = 0.5$ small deviation between new theoretical formula (47) and simulation data is observed in the range of magnetic field $1 \leq \alpha \leq 2$.

The typical behavior of the magnetization can be described as follows: the increasing of σ leads to the increasing of the magnetization in parallel case and decreasing the same in perpendicular configuration. This fact is clear illustrated in Fig. 9 where the simulation snapshots are given for model system with $\lambda_e = 0.5$ and $\alpha = 1$. Fig. 9 (a) corresponds the case when $\sigma = 0$ and scalar magnetization is equal to $M = 0.45$. The presence of easy axis with $\sigma = 5$ along the external magnetic field leads to an increase in scalar magnetization almost twice, that is shown in Fig. 9 (b). Perpendicular configuration with $\sigma = 5$ is given in Fig. 9 (c), where the magnetic response of the system on the external magnetic field is very weak. In this case the magnetic moments formed chains in the direction of easy axis so that the scalar magnetization in direction of \hat{n}_i is equal to zero, although a pronounced regular structure of the magnetic moments of all particles in the system is not yet observed for these parameters of the system.

The initial slope of magnetization curve is characterized by the initial magnetic susceptibility, which can be determined via the Helmholtz free energy as

$$\chi = \chi_{\text{id}} - \frac{1}{V} \left. \frac{\partial^2 \Delta F}{\partial H^2} \right|_{H=0}. \quad (48)$$

The comparison between theoretical predictions of χ and MC results is given in Fig. 10. Results are shown for both parallel and perpendicular configurations. As for ideal approximations (46), there are a significant discrepancy between dashed curves and simulation data in all considered systems, for parallel configuration especially. Even for weakly interacting system with $\lambda_e = 0.1$, that corresponds Fig. 10 (a), the difference between susceptibilities of the non-interacting (red dashed line) and interacting particles (red solid line) for parallel configuration is surprisingly large. Interactions lead a quick growth of susceptibility, and new theory (48) allows to accurately describe this behavior of χ_{\parallel} . One can note the good agreement between new theory (solid lines) and MC data (symbols) for both parallel and perpendicular configurations at $\lambda_e = 0.1$. With increasing of λ_e up to 0.3 in

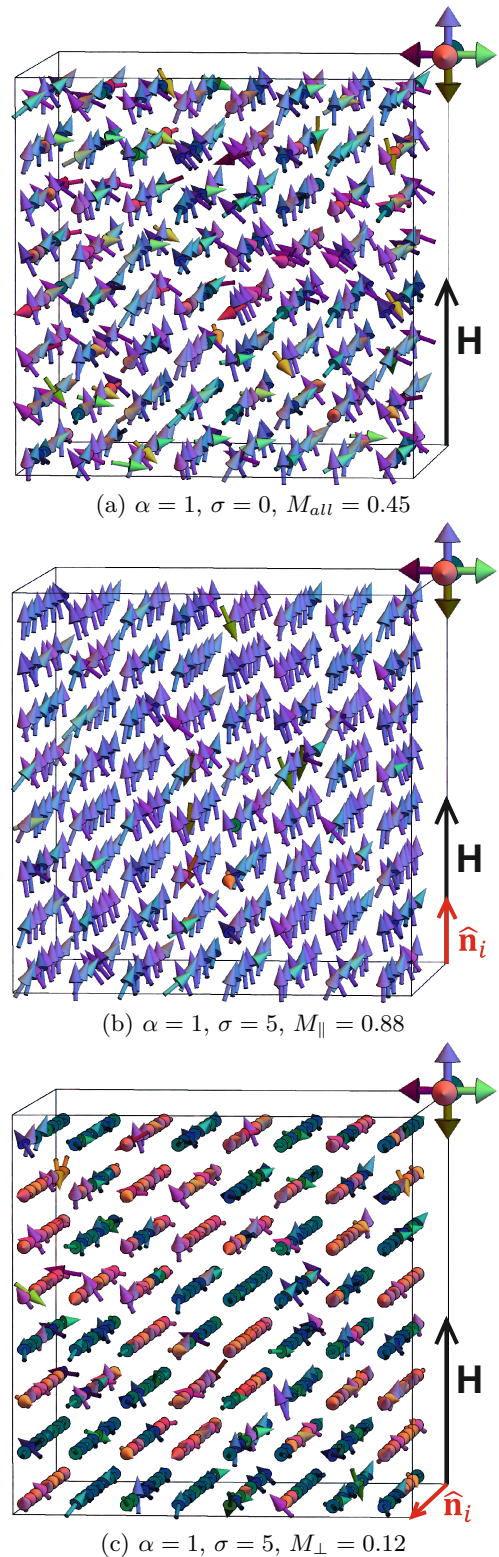


FIG. 9. Simulation snapshots of the model system with $\lambda_e = 0.5$ and $\alpha = 1$. Results are shown for (a) $\sigma = 0$, (b) parallel configurations with $\sigma = 5$ and (c) perpendicular configurations with $\sigma = 5$. Different arrow colors correspond to different orientations of the magnetic moments.

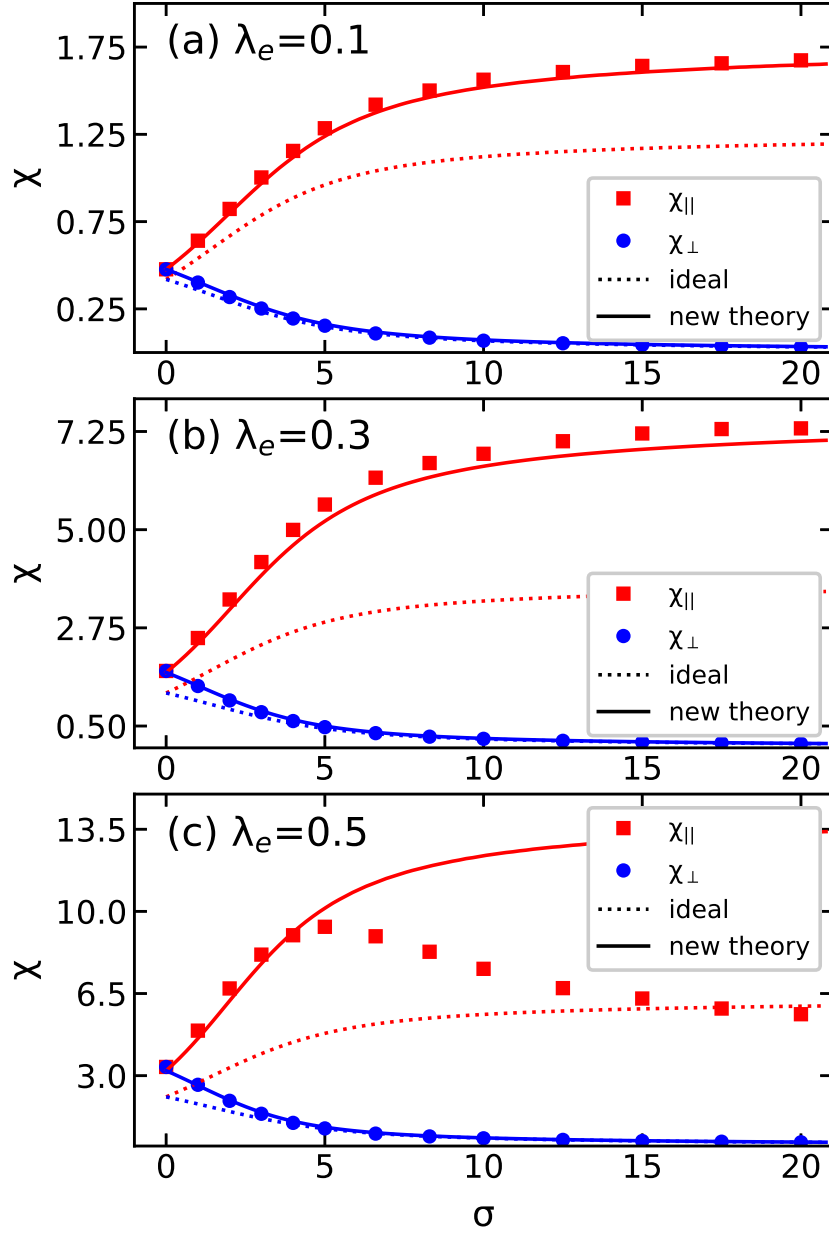


FIG. 10. The initial magnetic susceptibility χ as a function of the anisotropy parameter σ for systems with (a) $\lambda_e = 0.1$, (b) 0.3 and (c) 0.5. Solid lines correspond new theories for $\chi_{||}$ and χ_{\perp} , dashed lines are ideal approximation (46). Symbols are from Monte-Carlo simulations. Results are shown for parallel (red squares and lines) and perpendicular (blue circles and lines) configurations.

Fig. 10 (b), small deviation between new theory (48) and simulation data appears in the parallel configuration (red color), while for the perpendicular configuration (blue color), the agreement of theoretical and numerical results is still good. The MC results for the parallel configuration at $\lambda_e = 0.5$ (Fig. 10 (c)) demonstrate unexpectedly effect: non-monotonic behavior of susceptibility with increasing of σ . Note that the maximum achievable susceptibility value in this case is $\chi_{||} \simeq 9$ at $\sigma \simeq 5$. The potential reason of this behavior is that the total magnetic moment of system decreases due to appearance

of magnetically compensated structures. This suggestion can be confirmed from a visual examination of the simulation snapshots given in Fig. 11. The viewing angle on the system is changed to more clarity, so, that the blue vectors correspond to the direction of the Oz axis. All systems have a high value of the anisotropy parameter $\sigma = 20$, that leads to a rigid alignment of the magnetic moments along the easy axes. For system with $\lambda_e = 0.3$ (Fig. 11 (a)), there are no regular structures in magnetic moments' direction: snapshot contains many possible variants of alignment of magnetic moments in inner

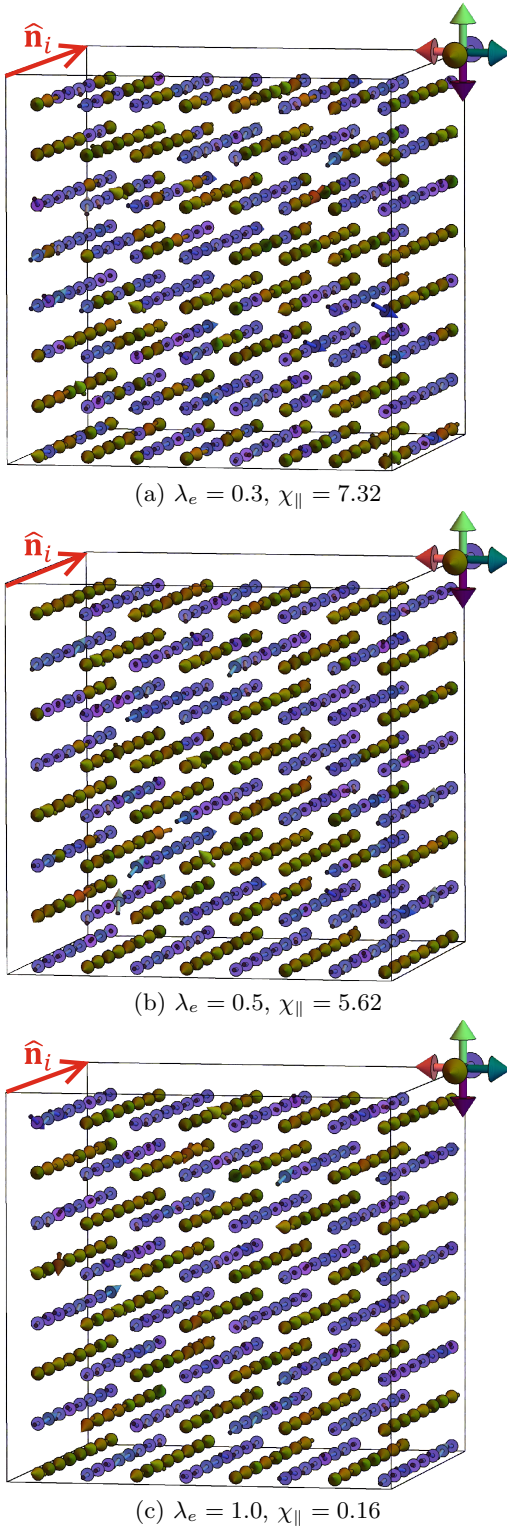


FIG. 11. Simulation snapshots of the model system with $\alpha = 0$ and $\sigma = 20$. Results are shown for parallel configurations with (a) $\lambda_e = 0.3$, (b) $\lambda_e = 0.5$ and (c) $\lambda_e = 1.0$. Different arrow colors correspond to different orientations of magnetic moments. The viewing angle on the system is changed to more clarity.

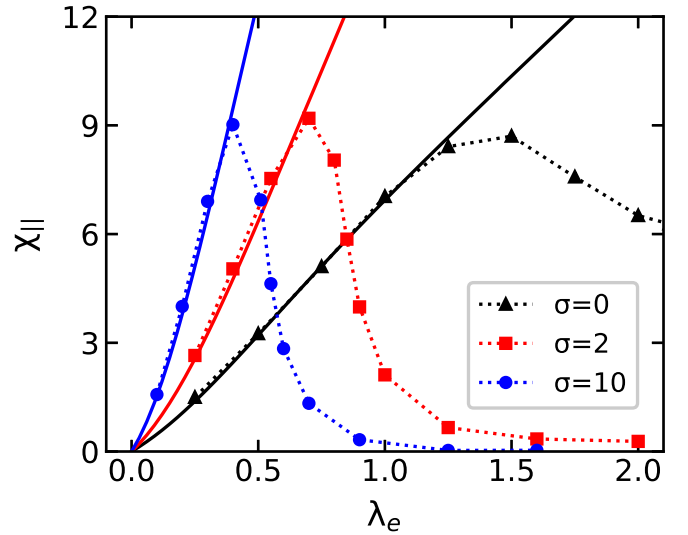


FIG. 12. The initial magnetic susceptibility χ_{\parallel} as a function of the parameter λ_e for parallel configuration. Solid lines correspond new theory for χ_{\parallel} . Symbols are from the Monte-Carlo simulations. Results are shown for systems with $\sigma = 0$ (black triangles and lines), $\sigma = 2$ (red squares and lines) and $\sigma = 10$ (blue circles and lines).

chains along easy axis. Fig. 11 (b) shows that for system with $\lambda_e = 0.5$ it is possible to note the pronounced way of arrangement of magnetic moments in chains along the easy axes: these are directed mainly in one direction within a single chain. Increasing the intensity of dipole interactions up to $\lambda_e = 1$ (Fig. 11 (c)), we have additional tendency in antiparallel alignment of chains along the easy axes, which as a result leads to a further decrease in the system's susceptibility. This case requires some discussion. Any chain parallel to \hat{n}_i in Fig. 11 (c) has four antiparallel nearest neighbors, that leads to a clear checkerboard pattern in the plane perpendicular to \hat{n}_i . For a single particle it is possible to conclude the following observations about its six nearest neighbors: two of them tend to adopt the most favorable “head-to-tail” orientation and the other four tend to adopt the second most favorable “side-by-side” orientation. Magnetic response of such system turns out very weak and needs the strong applied magnetic field to get the magneto-active material.

From Fig. 11 one can conclude that the dependency of χ_{\parallel} as a function of λ_e at the fixed value of σ also has non-monotonic type. This fact was observed in Ref. [24] at $\sigma = 0$ and the Molecular Dynamic simulation results are denoted in Fig. 12 by black symbols with dashed black curve. It should be noted the excellent agreement between new theory (48) and simulation data up to $\lambda_e \sim 1.25$, when there are no structural transformations in magnetic systems. The further increasing of the interaction intensity leads to the decreasing of susceptibility, the reason of which is specific nature of the orientational ordering: all dipoles tend to align in

long antiparallel chains spanning across the simulation box. During the current investigation, the dependency of χ_{\parallel} as a function of λ_e was calculated for systems with easy axis, anisotropy parameters of which had the values $\sigma = 2$ and 10 . The obtained MC results are denoted in Fig. 12 as red symbols with dashed red curve and blue symbols with dashed blue curve respectively. The increasing of σ causes a shift of the susceptibility maximum to left. One can see that the value of this shift from $\sigma = 0$ to 2 turns out bigger than the same from $\sigma = 2$ to 10 . Also it worse be stressed that the susceptibility fall begins when the value $\chi_{\parallel} \simeq 9$ is reached regardless of the value of the anisotropy parameter σ . This is consistent with the results from the Fig. 10 (c): susceptibility increases with increasing of σ up to the value of $\chi_{\parallel} \simeq 9$ and decreases further. This fact allows to conclude that the model system of ferroparticles can demonstrate the maximum value of susceptibility in parallel configuration $\chi_{\parallel} \simeq 9$, and it is the inner property of considered way of ferroparticles placement at the nodes of the simple cubic lattice. It should be emphasized that in a system of interacting immobilized superparamagnetic particles located randomly, the pronounced regular structuring of the magnetic moments of particles is not observed for the parameters under consideration [17].

New theory is able to predict the magnetic properties of the model system in the range of parameters λ_e and σ , for which the susceptibility value turns out $\chi_{\parallel} \leq 9$ and there are no regular structuring of the particle's magnetic moment in the systems. To clarify this range, it is possible to plot the phase diagram using the MC data from Fig. 10

- at $\lambda_e = 0.3$ new theory works well up to $\sigma = 20$,
- at $\lambda_e = 0.5$ new theory works well up to $\sigma = 5$,

and from Fig. 12

- at $\sigma = 0$ new theory works well up to $\lambda_e = 1.25$,
- at $\sigma = 2$ new theory works well up to $\lambda_e = 0.7$,
- at $\sigma = 10$ new theory works well up to $\lambda_e = 0.4$.

The range of the applicability of the new theory is denoted as grey area in Fig. 13. The area above dashed line indicates on the ordered state with the presence of ferromagnetic chains arranged antiferromagnetically in zero fields, that leads to the susceptibility decreasing. Antiferromagnetic ordering of the magnetic moments was also discovered in the study of the ground state of a simple cubic lattice of dipoles in a zero field in Ref. [39].

The deviation of new theory from the results of computer modeling in Figs. 10 (c), 12 is connected with the limitation in the Helmholtz free energy (36), (41) by the second virial coefficient and the third power of the effective dipolar coupling constant. Increasing the number of terms in the virial series could expand the scope of new theory. However, using the virial expansion approach it is quite difficult to obtain the theory that is valid for

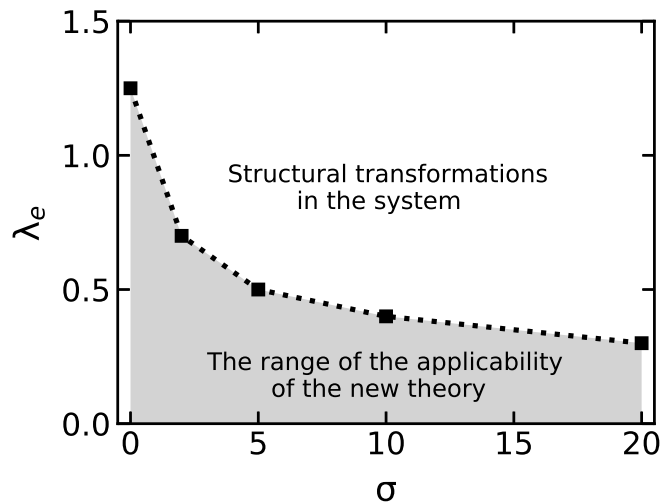


FIG. 13. The phase diagram of the uniaxial superparamagnetic nanoparticles embedded in simple cubic lattice. Grey area corresponds the state of system without regular structuring of the particle's magnetic moments, where the new theory (48), (36), (41) is able to describe the magnetic properties of the model.

the systems with strong dipolar regime. In this case, an alternative method can be used, for instance [40, 41].

IV. CONCLUSION

The static magnetic response of the interacting superparamagnetic ferroparticles embedded in a simple cubic lattice has been studied by theory and simulation. The potential energy of the system has included one-particle dipole-easy axis interaction, one-particle dipole-field interaction, and long-range interparticle dipole-dipole interactions. Two orientational distributions of particle's easy axis in the system have been considered: aligned parallel and perpendicular to the direction of an external magnetic field. For both cases, the analytical expression for the Helmholtz free energy in logarithmic form has been derived considering pairwise dipole-dipole interactions from the rigorous methods of statistical physics. Using the obtained formula for the Helmholtz free energy, the scalar magnetization and the initial magnetic susceptibility have been investigated in the broad range of parameters. The theoretical predictions have been critically compared with MC simulation data.

For parallel configuration, the magnetic moments are preferably aligned along the direction of the field, that provides the strong magnetic enhancement. For perpendicular configuration, the magnetic moments are held by the easy axes in the direction of perpendicular to the field and magnetization decreases with grows of anisotropy parameter σ . In both cases, the interparticle dipole-dipole interactions lead to an increase of magnetization, but this enhancement is much stronger for the parallel configura-

tion. The ideal approach is not capable to describe the simulation data adequately, whereas the theory derived in this paper turned out much more efficient.

The susceptibility curves from MC simulations have demonstrated several interesting results. Firstly, non-monotonic behavior of χ_{\parallel} has been observed with increasing of anisotropy parameter or the dipole-dipole interaction intensity. Notice, that for a system of interacting immobilized superparamagnetic particles located randomly, the initial magnetic susceptibility increases monotonically with growth of anisotropy parameter or the dipole-dipole interaction intensity [17]. Secondly, for any set of intrinsic parameters, the maximum achievable value of χ_{\parallel} has been equal to $\simeq 9$. This allows us to conclude that the model system based on the simple cubic lattice undergoes a phase transition in the ordering of magnetic moments. There has been determined the area of parameters λ_e and σ , where structural transformations are absent. In this area, the theoretic susceptibility curves turned out in the good agreement with MC data. The obtained results about magnetic properties of the simple cubic lattice with the immobilized superparamagnetic nanoparticles in nodes is important in the development of functional magnetic materials with controlled properties.

ACKNOWLEDGEMENTS

The reported study was funded by RFBR, project number 20-02-00358.

APPENDIX A: PARALLEL CONFIGURATION

For parallel configuration the results of the averaging over magnetic moment orientations of the coefficients b_1 , b_2 , b_3 can be written in the following form

$$b_1 = 2Q_1^2(\alpha, \sigma)\gamma_{12}, \quad (\text{A.1})$$

$$b_2 = \frac{36}{35}Q_2^2(\alpha, \sigma)\gamma_{24} + \frac{2}{3}Q_2(\alpha, \sigma) \left(1 - \frac{Q_2(\alpha, \sigma)}{7}\right)\gamma_{22} + \frac{1}{3} \left(1 + \frac{Q_2^2(\alpha, \sigma)}{5}\right)\gamma_{20}, \quad (\text{A.2})$$

$$b_3 = \frac{6}{77}(3Q_1(\alpha, \sigma) - 5Q_3(\alpha, \sigma))^2\gamma_{36} + \frac{18}{11} \left(\frac{4Q_1(\alpha, \sigma)Q_3(\alpha, \sigma)}{5} - \frac{3Q_1^2(\alpha, \sigma)}{7}\right) - \frac{Q_3^2(\alpha, \sigma)}{7}\gamma_{34} + \frac{1}{7}(3Q_1^2(\alpha, \sigma) + Q_3^2(\alpha, \sigma))\gamma_{32} + \frac{1}{42} \left(\frac{6Q_1(\alpha, \sigma)Q_3(\alpha, \sigma)}{5} + 3Q_1^2(\alpha, \sigma) - Q_3^2(\alpha, \sigma)\right)\gamma_{30}, \quad (\text{A.3})$$

where several functions have been introduced as

$$Q_1(\alpha, \sigma) = \frac{1}{2Q_0(\alpha, \sigma)} \int_{-1}^1 \exp(\alpha t + \sigma t^2) t dt, \quad (\text{A.4})$$

$$Q_1(\alpha, 0) = L(\alpha),$$

$$L(\alpha) = \coth \alpha - \frac{1}{\alpha},$$

$$Q_2(\alpha, \sigma) = -\frac{1}{2} + \frac{3}{4Q_0(\alpha, \sigma)} \int_{-1}^1 \exp(\alpha t + \sigma t^2) t^2 dt, \quad (\text{A.5})$$

$$Q_2(\alpha, 0) = L_3(\alpha),$$

$$L_3(\alpha) = 1 - 3\frac{L(\alpha)}{\alpha},$$

$$Q_3(\alpha, \sigma) = \frac{1}{2Q_0(\alpha, \sigma)} \int_{-1}^1 \exp(\alpha t + \sigma t^2) t^3 dt, \quad (\text{A.6})$$

$$Q_3(\alpha, 0) = L(\alpha) - \frac{2}{\alpha}L_3(\alpha).$$

The numbers γ_{pq} involve the summation of position depended expressions over nodes of the cubic lattice, limited by cylinder size:

$$\gamma_{pq} = \sum_{j=2}^N \frac{1}{\tilde{r}_{1j}^{3p}} P_q \left(\frac{\tilde{z}_{1j}}{\tilde{r}_{1j}} \right), \quad (\text{A.7})$$

where P_q ($q = 0, 2, 4, 6$) are the Legendre polynomials, $\tilde{\mathbf{r}}_{1j} = \mathbf{r}_{1j}/a$ is a dimensionless center-center vector, \tilde{z}_{1j} is z -component of vector $\tilde{\mathbf{r}}_{1j}$ in a coordinate system, illustrated in Fig. 1 (a). It is assumed that particle 1 is fixed at the origin of the laboratory coordinate system, meaning $(\tilde{x}_1, \tilde{y}_1, \tilde{z}_1) \equiv (0, 0, 0)$. The coordinates of particle j in this case can be located in all the other nodes of the simple cubic lattice, limited by cylinder size:

$$\begin{aligned} -R &\leq \tilde{x}_j \leq R, \\ -R &\leq \tilde{y}_j \leq R, \\ -hR &\leq \tilde{z}_j \leq hR, \\ (\tilde{x}_j)^2 + (\tilde{y}_j)^2 &\leq R^2, \\ (\tilde{x}_j)^2 + (\tilde{y}_j)^2 + (\tilde{z}_j)^2 &> 0. \end{aligned} \quad (\text{A.8})$$

where R is the dimensionless radius of the cylinder and h is the factor describing the cylinder elongation. The results for γ_{pq} obtained for model system with $N \simeq 25 \times 10^6$ ferroparticles are $\gamma_{12} = 2.0944$, $\gamma_{24} = 3.2257$, $\gamma_{22} = \gamma_{32} = 0$, $\gamma_{20} = 8.4016$, $\gamma_{36} = 0.6553$, $\gamma_{34} = 3.4081$, $\gamma_{30} = 6.6289$.

APPENDIX B: PERPENDICULAR CONFIGURATION

For perpendicular configuration the results of the averaging over magnetic moment orientations of the coefficients b_1 , b_2 , b_3 can be written in the following form

$$b_1 = 2R_1^2(\alpha, \sigma)\epsilon_1, \quad (\text{B.1})$$

$$b_2 = (R_2^2(\alpha, \sigma) + 3R_3^2(\alpha, \sigma) - 2R_3(\alpha, \sigma) + 1)\epsilon_2 \\ + \frac{9}{4}(2R_3(\alpha, \sigma) - 3R_3^2(\alpha, \sigma) - R_2^2(\alpha, \sigma) + 1)\epsilon_3, \quad (\text{B.2})$$

$$b_3 = \frac{4}{3}R_5^2(\alpha, \sigma)\epsilon_4 \\ + 4[(R_4(\alpha, \sigma) - R_5(\alpha, \sigma))^2 + R_6^2(\alpha, \sigma)]\epsilon_5 \\ + 18[R_4^2(\alpha, \sigma) + R_6^2(\alpha, \sigma) + R_5(\alpha, \sigma)R_6(\alpha, \sigma) \\ - R_4(\alpha, \sigma)R_5(\alpha, \sigma)]\epsilon_6 \\ + 9(R_4(\alpha, \sigma) - R_5(\alpha, \sigma))R_6(\alpha, \sigma)\epsilon_7, \quad (\text{B.3})$$

where additional functions have been introduced as

$$R_1(\alpha, \sigma) = \int_0^1 \exp(\sigma t^2) I_0(\alpha\sqrt{1-t^2})\sqrt{1-t^2} dt \\ \times \frac{1}{R_0(\alpha, \sigma)}, \quad (\text{B.4})$$

$$R_1(\alpha, 0) = L(\alpha),$$

$$R_2(\alpha, \sigma) = \int_0^1 \exp(\sigma t^2) I_2(\alpha\sqrt{1-t^2})(1-t^2) dt \\ \times \frac{1}{R_0(\alpha, \sigma)}, \quad (\text{B.5})$$

$$R_2(\alpha, 0) = L_3(\alpha),$$

$$R_3(\alpha, \sigma) = \frac{1}{R_0(\alpha, \sigma)} \int_0^1 \exp(\sigma t^2) I_0(\alpha\sqrt{1-t^2})t^2 dt, \quad (\text{B.6})$$

$$R_3(\alpha, 0) = \frac{L(\alpha)}{\alpha},$$

$$R_4(\alpha, \sigma) = \int_0^1 \exp(\sigma t^2) I_1(\alpha\sqrt{1-t^2})\sqrt{1-t^2}^3 dt \\ \times \frac{1}{R_0(\alpha, \sigma)}, \quad (\text{B.7})$$

$$R_4(\alpha, 0) = L(\alpha) - \frac{L_3(\alpha)}{\alpha},$$

$$R_5(\alpha, \sigma) = \int_0^1 \exp(\sigma t^2) I_3(\alpha\sqrt{1-t^2})\sqrt{1-t^2}^3 dt \\ \times \frac{1}{R_0(\alpha, \sigma)}, \quad (\text{B.8})$$

$$R_5(\alpha, 0) = L(\alpha) - 2\frac{L_3(\alpha)}{\alpha},$$

$$R_6(\alpha, \sigma) = \int_0^1 \exp(\sigma t^2) I_1(\alpha\sqrt{1-t^2})\sqrt{1-t^2}t^2 dt \\ \times \frac{1}{R_0(\alpha, \sigma)}, \quad (\text{B.9})$$

$$R_6(\alpha, 0) = \frac{L_3(\alpha)}{\alpha}.$$

Here $I_k(x)$ is the modified Bessel function of k order, the numbers ϵ_k involve the summation of position depended expressions over nodes of the cubic lattice, limited by cylinder size:

$$\epsilon_1 = \sum_{j=2}^N \frac{1}{\tilde{r}_{1j}^3} P_2\left(\frac{\tilde{x}_{1j}}{\tilde{r}_{1j}}\right) \simeq 2.0944, \quad (\text{B.10})$$

$$\epsilon_2 = \sum_{j=2}^N \frac{1}{\tilde{r}_{1j}^6} P_2^2\left(\frac{\tilde{x}_{1j}}{\tilde{r}_{1j}}\right) \simeq 3.3393, \quad (\text{B.11})$$

$$\epsilon_3 = \sum_{j=2}^N \frac{\tilde{x}_{1j}^2 \tilde{z}_{1j}^2}{\tilde{r}_{1j}^{10}} \simeq 0.1915, \quad (\text{B.12})$$

$$\epsilon_4 = \sum_{j=2}^N \frac{1}{\tilde{r}_{1j}^9} P_2^3\left(\frac{\tilde{x}_{1j}}{\tilde{r}_{1j}}\right) \simeq 1.4880, \quad (\text{B.13})$$

$$\epsilon_5 = \sum_{j=2}^N \frac{1}{\tilde{r}_{1j}^9} P_2\left(\frac{\tilde{x}_{1j}}{\tilde{r}_{1j}}\right) P_2^2\left(\frac{\tilde{z}_{1j}}{\tilde{r}_{1j}}\right) \simeq -0.7440, \quad (\text{B.14})$$

$$\epsilon_6 = \sum_{j=2}^N \frac{\tilde{x}_{1j}^2 \tilde{z}_{1j}^2}{\tilde{r}_{1j}^{13}} P_2\left(\frac{\tilde{z}_{1j}}{\tilde{r}_{1j}}\right) \simeq 0.0114, \quad (\text{B.15})$$

$$\epsilon_7 = \sum_{j=2}^N \frac{\tilde{y}_{1j}^2 \tilde{z}_{1j}^2 (8\tilde{x}_{1j}^2 - \tilde{y}_{1j}^2 - \tilde{z}_{1j}^2)}{\tilde{r}_{1j}^{15}} \simeq -0.0318. \quad (\text{B.16})$$

[1] G. Steinbach, M. Schreiber, D. Nissen, M. Albrecht, E. Novak, P.A. Sanchez, S.S. Kantorovich, S. Gemming, and A. Erbe, "Field-responsive colloidal assemblies defined by magnetic anisotropy," *Physical Review E* **100**, 012608 (2019).
[2] I.E. Kuznetsova, V.V. Kolesov, A.S. Fionov, E.Y. Kramarenko, G.V. Stepanov, M.G. Mikheev, E. Verona, and I. Solodov, "Magnetoactive elastomers with controllable radio-absorbing properties," *Materials Today Communications* **21**, 100610 (2019).
[3] D. Borin, G. Stepanov, and E. Dohmen, "Hybrid magnetoactive elastomer with a soft matrix and mixed powder," *Archive of Applied Mechanics* **89**, 105–117 (2019).

[4] G. Filipcsei, I. Csetneki, A. Szilágyi, and M. Zrínyi, "Magnetic field-responsive smart polymer composites," *Advances in Polymer Science*, **206**, 137–189 (2007).
[5] S. Dutz and R. Hergt, "Magnetic nanoparticle heating and heat transfer on a microscale: Basic principles, realities and physical limitations of hyperthermia for tumour therapy," *International Journal of Hyperthermia* **29**, 790–800 (2013).
[6] D. Ortega and Q. A. Pankhurst, "Magnetic hyperthermia," *Nanoscience* **1**, 60–88 (2013).
[7] A.Yu. Zubarev, "Magnetic hyperthermia in a system of ferromagnetic particles, frozen in a carrier medium: Effect of interparticle interactions," *Physical Review E* **98**,

- 032610 (2018).
- [8] A.Yu. Zubarev, “Magnetic hyperthermia in a system of immobilized magnetically interacting particles,” *Physical Review E* **99**, 062609 (2019).
 - [9] Yu.L. Raikher and M.I. Shliomis, “Theory of dispersion of the magnetic susceptibility of fine ferromagnetic particles,” *Journal of Experimental and Theoretical Physics* **40**, 526532 (1974).
 - [10] M.I. Shliomis and V.I. Stepanov, “Theory of the dynamic susceptibility of magnetic fluids,” *Advances in Chemical Physics* **87**, 130 (1994).
 - [11] S.A. Shah, D.B. Reeves, R.M. Ferguson, J.B. Weaver, and K.M. Krishnan, “Mixed brownian alignment and neel rotations in superparamagnetic iron oxide nanoparticle suspensions driven by an ac field,” *Physical Review B* **92**, 094438 (2015).
 - [12] A.Yu. Gervald, I.A. Gritskova, and N.I. Prokopov, “Synthesis of magnetic polymeric microspheres,” *Russian Chemical Reviews* **79**, 219–229 (2010).
 - [13] H.H. Valiev, A. Ya Minaev, G.V. Stepanov, and Y.N. Karnet, “Study of filler microstructure in magnetic soft composites,” *Journal of Physics: Conference Series* **1260**, 112034 (2019).
 - [14] V. Ganesan, B.B. Lahiri, C. Louis, J. Philip, and S.P. Damodaran, “Size-controlled synthesis of superparamagnetic magnetite nanoclusters for heat generation in an alternating magnetic field,” *Journal of Molecular Liquids* **281**, 315–323 (2019).
 - [15] A. Zakinyan and I. Arefyev, “Thermal conductivity of emulsion with anisotropic microstructure induced by external field,” *Colloid and Polymer Science* **298**, 10631076 (2020).
 - [16] T. Yoshida, Y. Matsugi, N. Tsujimura, T. Sasayama, K. Enpuku, T. Viereck, M. Schilling, and F. Ludwig, “Effect of alignment of easy axes on dynamic magnetization of immobilized magnetic nanoparticles,” *Journal of Magnetism and Magnetic Materials* **427**, 162–167 (2017).
 - [17] E.A. Elfimova, A.O. Ivanov, and P.J. Camp, “Static magnetization of immobilized, weakly interacting, superparamagnetic nanoparticles,” *Nanoscale* **11**, 21834–21846 (2019).
 - [18] V. Socoliuc and L.B. Popescu, “Determination of the statistics of magnetically induced particle chains in concentrated ferrofluids,” *Journal of Magnetism and Magnetic Materials* **502**, 166532 (2020).
 - [19] A.S. Elkady, L. Iskakova, and A. Zubarev, “On the self-assembly of net-like nanostructures in ferrofluids,” *Physica A: Statistical Mechanics and its Applications* **428**, 257–265 (2015).
 - [20] A. Sreekumari and P. Ilg, “Slow relaxation in structure-forming ferrofluids,” *Physical Review E - Statistical, Nonlinear, and Soft Matter Physics* **88**, 042315 (2013).
 - [21] A.F. Pshenichnikov and A.S. Ivanov, “Magnetophoresis of particles and aggregates in concentrated magnetic fluids,” *Physical Review E - Statistical, Nonlinear, and Soft Matter Physics* **86**, 051401 (2012).
 - [22] P. Ilg, “Equilibrium magnetization and magnetization relaxation of multicore magnetic nanoparticles,” *Physical Review B* **95**, 214427 (2017).
 - [23] A.F. Pshenichnikov and A.A. Kuznetsov, “Self-organization of magnetic moments in dipolar chains with restricted degrees of freedom,” *Physical Review E - Statistical, Nonlinear, and Soft Matter Physics* **92**, 042303 (2015).
 - [24] A. Yu. Solovyova, A. A. Kuznetsov, and E. A. Elfimova, “Correlations in the simple cubic lattice of ferroparticles: Theory and computer simulations,” *Physica A* **558**, 124923 (2020).
 - [25] E.A. Elfimova, A.O. Ivanov, L.B. Popescu, and V. Socoliuc, “Transverse magneto-optical anisotropy in bidisperse ferrofluids with long range particle correlations,” *Journal of Magnetism and Magnetic Materials* **431**, 54–58 (2017).
 - [26] T.M. Batrudinov, Yu.E. Nekhoroshkova, E.I. Paramonov, V.S. Zverev, E.A. Elfimova, and A.O. Ivanov, “Dynamic magnetic response of a ferrofluid in a static uniform magnetic field,” *Physical Review E* **052602**, 052602 (2018).
 - [27] A.O. Ivanov and P.J. Camp, “Theory of the dynamic magnetic susceptibility of ferrofluids,” *Physical Review E* **98**, 050602 (2018).
 - [28] A.Y. Solovyova, E.A. Elfimova, A.O. Ivanov, and P.J. Camp, “Modified mean-field theory of the magnetic properties of concentrated, high-susceptibility, polydisperse ferrofluids,” *Physical Review E* **96**, 052609 (2017).
 - [29] A.V. Nagornyi, V. Socoliuc, V.I. Petrenko, L. Almasy, O.I. Ivankov, M.V. Avdeev, L.A. Bulavin, and L. Vekas, “Structural characterization of concentrated aqueous ferrofluids,” *Journal of Magnetism and Magnetic Materials* **501**, 166445 (2020).
 - [30] A.V. Lebedev, V.I. Stepanov, A.A. Kuznetsov, A.O. Ivanov, and A.F. Pshenichnikov, “Dynamic susceptibility of a concentrated ferrofluid: The role of interparticle interactions,” *Physical Review E* **100**, 032605 (2019).
 - [31] F. Pousaneh and A.S. De Wijn, “Kinetic theory and shear viscosity of dense dipolar hard sphere liquids,” *Physical Review Letters* **124**, 218004 (2020).
 - [32] R. Balescu, *Equilibrium and nonequilibrium statistical mechanics* (Wiley, 1975).
 - [33] D. Henderson, “Some simple results for the properties of polar fluids,” *Condensed Matter Physics* **14**, 33001 (2011).
 - [34] C.G. Joslin, “The third dielectric and pressure virial coefficients of dipolar hard sphere fluids,” *Molecular Physics* **42**, 1507–1518 (1981).
 - [35] E.A. Elfimova, A.O. Ivanov, and P.J. Camp, “Thermodynamics of dipolar hard spheres with low-to-intermediate coupling constant,” *Physical Review E* **86**, 021126 (2012).
 - [36] E.A. Elfimova, A.O. Ivanov, and P.J. Camp, “Thermodynamics of ferrofluids in applied magnetic fields,” *Physical Review E* **88**, 042310 (2013).
 - [37] A.Yu. Solovyova and E.A. Elfimova, “The initial magnetic susceptibility of high-concentrated, polydisperse ferrofluids: universal theoretical expression,” *Journal of Magnetism and Magnetic Materials* **495**, 165846 (2020).
 - [38] M. P. Allen and D. J. Tildesley, *Computer simulation of liquids* (Clarendon Press, Oxford, 1987).
 - [39] R. Kretschmer and K. Binder, “Ordering and phase transitions in ising systems with competing short range and dipolar interactions,” *Zeitschrift für Physik B Condensed Matter* **34**, 375–392 (1979).
 - [40] Y.A. Budkov and M.G. Kiselev, “Flory-type theories of polymer chains under different external stimuli,” *Journal of Physics Condensed Matter* **30**, 043001 (2018).
 - [41] Yu.A. Budkov and A.L. Kolesnikov, “On a new application of the path integrals in polymer statistical physics,” *Journal of Statistical Mechanics: Theory and Experiment* **2016**, 103211 (2016).